Showcasing research from VTT Technical Research Centre of Finland and University of Oulu, Finland.

Mechanochemical synthesis of Pt/TiO$_2$ for enhanced stability in dehydrogenation of methylcyclohexane

Metallic platinum was supported on titania by simple and waste-free dry ball milling method, and the Pt/TiO$_2$ catalyst was studied in continuous-flow dehydrogenation of methylcyclohexane. Detailed catalyst characterisation showed that ball milling produced well-dispersed Pt nanoparticles, and furthermore, the high-energy milling induced phase transformation of the titania support. The mechanochemically synthesised catalyst provided a high hydrogen productivity rate (670 mmol $_{H2}$/(g$_{Pt}$*min)) and improved selectivity and stability compared to a corresponding catalyst prepared by conventional wet synthesis method.

Image reproduced by permission of Krista Kuutti from *Catal. Sci. Technol.*, 2025, **15**, 4143.

ROYAL SOCIETY OF **CHEMISTRY**

rsc.li/catalysis

Check for updates

Mechanochemical synthesis of Pt/TiO$_2$ for enhanced stability in dehydrogenation of methylcyclohexane†

Krista Kuutti, [iD] [a] Manoj Kumar Ghosalya, [iD] [b] Paavo Porri,[a] Jacopo De Bellis, [iD] ‡[c]
Päivi Jokimies,[a] Harishchandra Singh, [iD] [b] Shubo Wang, [iD] [b] Graham King, [iD] [d]
Javier Fernández-Catalá,[be] Ferdi Schüth,[c] Kaisu Ainassaari, [iD] [f] Mika Huuhtanen, [iD] [f]
Marko Huttula, [iD] [b] Samuli Urpelainen [iD] *[b] and Sari Rautiainen [iD] *[a]

Catalytic hydrogenation/dehydrogenation of liquid organic hydrogen carriers (LOHCs), such as methylcyclohexane (MCH), enables versatile and safe transport and storage of hydrogen as a carbon neutral fuel. Supported platinum catalysts are commonly used for the dehydrogenation reaction, however, they often suffer from loss of activity due to coking. Herein, we present mechanochemically synthesised platinum on titania catalyst for the dehydrogenation of MCH, prepared starting only from metallic platinum and titania. Dry mechanochemical catalyst syntheses do not produce waste waters or toxic fumes, which are generated in the deposition of metal precursors by conventional wet synthesis methods. Detailed characterisation of the catalysts revealed that ball milling produced highly dispersed nanoparticles. Furthermore, continuous-flow MCH dehydrogenation experiments showed that the mechanochemically prepared Pt catalyst exhibited improved selectivity and stability compared to a conventional impregnated Pt/TiO$_2$ catalyst. The hydrogen production rate of the novel ball-milled catalyst was among the highest reported for dehydrogenation of methylcyclohexane, 670 mmol$_{H_2}$ g$_{Pt}^{-1}$ min^{-1}.
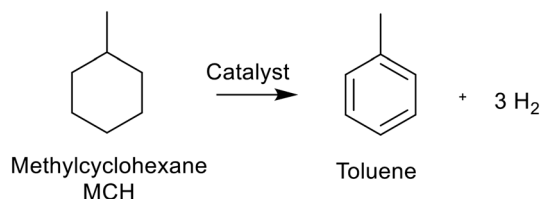
1 Introduction

Green hydrogen produced *via* water splitting using renewable energy could serve as a carbon neutral fuel.[1] High energy density is essential for a fuel, and H$_2$ possesses the highest gravimetric energy density of all energy carriers, 120 MJ kg^{-1}. For comparison, the corresponding value for gasoline is ~40 MJ kg^{-1}.[2] The volumetric energy density of ambient H$_2$ gas, however, is very low

[a] *VTT Technical Research Centre of Finland Ltd, Espoo FI-02044, Finland.*
E-mail: sari.rautiainen@vtt.fi
[b] *Nano and Molecular Systems Research Unit, University of Oulu, 90014 Oulu,*
Finland. E-mail: samuli.urpelainen@oulu.fi
[c] *Department of Heterogeneous Catalysis, Max-Planck-Institut für Kohlenforschung,*
Kaiser-Wilhelm-Platz 1, 45470 Mülheim an der Ruhr, Germany
[d] *Canadian Light Source, 44 Innovation Boulevard, Saskatoon, Saskatchewan, S7N*
2V3 Canada
[e] *Materials Institute and Inorganic Chemistry Department, University of Alicante,*
Ap. 99, Alicante E-03080, Spain
[f] *Environmental and Chemical Engineering Research Unit, University of Oulu,*
90014 Oulu, Finland
† Electronic supplementary information (ESI) available. See DOI: https://doi.org/10.1039/d5cy00173k
‡ Present address: Department of Sustainable Process & Energy Systems, Energy & Materials Transition Unit, TNO, Kesslerpark 1, 2288 GS Rijswijk, The Netherlands.

requiring a compaction method for its viable storage and transportation.[3] One promising H$_2$ compaction method is chemical bonding to a storage medium, such as liquid organic hydrogen carriers (LOHCs). LOHCs are mainly cycloalkanes/aromatic compounds, that can undergo reversible hydrogenation/dehydrogenation reactions in the presence of suitable catalysts. A well-performing LOHC should have relatively high H$_2$ storage capacity (6–8 wt%) and wide temperature range for the liquid state. The liquid form enables usage of existing pumping systems, fuel containers and transportation vehicles with just minor modifications. Notably, two LOHC systems have already been commercialised, namely methylcyclohexane/toluene by Chiyoda Corporation[2] and a technical mixture of benzyltoluenes by Hydrogenious.[3] For the present work, the methylcyclohexane/toluene system was selected for the experiments, being one of the most promising LOHC systems given its low toxicity and broad applicability to the conventional fuel distribution infrastructure.[4,5] Scheme 1 presents the endothermic $\left(\Delta H_2 = +205 \frac{kJ}{mol} \right)$[47] dehydrogenation reaction of MCH to toluene.

Industrially, aromatics are refined from crude oil *via* catalytic reforming, and cycloalkanes are manufactured by hydrogenating these oil-derived aromatics. In terms of LOHC technologies this means that there are commercial processes

This journal is © The Royal Society of Chemistry 2025

Catal. Sci. Technol., 2025, **15**, 4143–4155 | **4143**

Methylcyclohexane
MCH

Toluene

+ 3 H$_2$

Scheme 1 MCH dehydrogenation reaction.

and catalysts readily available for aromatic hydrogenation, but cycloalkane dehydrogenation technologies are not comparably established.[3] Cycloalkane dehydrogenation is an endothermic reaction that occurs at elevated temperatures (150–400 °C) and relatively low pressure (<10 bar) over a metal catalyst. The choice of catalyst is crucial for the process as it should enable numerous LOHC hydrogenation/dehydrogenation cycles with minimum side products formation.[4] While hydrogenation catalysts are well established, viable and stable catalysts for the dehydrogenation reaction are still under development.

Platinum is the most extensively studied metal catalyst for LOHC dehydrogenation due to its high selectivity and superior activity in the reaction.[4] Pt is often supported on high surface area alumina owing to the thermal stability of the support and the ability to maintain high dispersion of Pt nanoparticles.[6] However, the acid sites on alumina may lead to coking and deactivation of the catalyst. Different strategies have been suggested to reduce the excess acidity, for instance doping the catalyst with alkali metals.[7] Yang *et al.* modified the alumina support by deposition of titania to reduce the acidity, resulting in increased stability and conversion of MCH.[8] Another strategy is to use another support material altogether. Nagatake *et al.* studied MCH dehydrogenation over TiO$_2$ and Al$_2$O$_3$ supported Pt catalysts and detected significantly less coke formation over the TiO$_2$ supported catalyst.[5] Both studies suggested strong metal support interactions between Pt and the TiO$_2$ support may induce charge transfer from the support to Pt causing an electron rich state. Similar phenomenon was not detected with the Al$_2$O$_3$ supported Pt. Moreover, Pt/TiO$_2$ catalyst was shown to excel over alumina-supported one in the dehydrogenation of perhydrogenated dibenzyl toluene.[9] Interestingly, platinum supported on a mixture of rutile–anatase demonstrated higher activity in the reaction compared to its alumina-supported counterpart or Pt on pure anatase support.

Typically, the catalyst preparation is carried out using solution-based methods, *e.g.* precipitation and impregnation. These methods produce large amounts of waste and can have challenges in the reproducibility of the preparation. Recently, mechanochemical methods, such as ball milling have gained attention as easily reproducible, scalable and simple methods for heterogeneous catalyst preparation.[10] Generally, ball milling is a controllable, efficient, low cost, and green solid-state mechanical powder processing technique that is frequently used to fabricate equilibrium and/or non-

equilibrium phases with reduced crystallite size compared to initial ingredients.[11] Ball mill catalyst synthesis can be operated fully solvent-free and with high yield.[12] In a planetary ball mill, rotating movement of the jar causes the grinding balls to collide and rub against each other and the walls, exerting impact, shear and friction forces on the materials inside the jar. As a result, highly dispersed nano-sized particles can be obtained in a high energy ball mill, starting simply from support material and metal powder.[12,13] The harder material (oxide support) acts as a grinding body towards the softer material (metal) that is subjected to activation by deformation, leading to metal application on top of the oxide support.[14] Direct deposition of the metal instead of a metal containing precursor, such as nitrate or chloride, omits the need for an energy intensive calcination step that is required for the wet synthesis methods for precursor removal.

Mechanochemically prepared catalysts have been studied in various reactions, and many reports show similar or improved activities compared to conventionally prepared catalysts. For instance, ball-milled gold catalysts were tested in CO oxidation, and their performance was well in line with catalysts prepared by impregnation methods.[13] Comparison of ball-milled and impregnated cobalt catalysts in methane dry reforming showed that the mechanochemical synthesis improved the dispersion and stability of the active metal on the support, resulting in more active and stable catalysts compared to the impregnated ones.[15] These interesting results prompted us to investigate the use of ball milling for the preparation of platinum catalysts for dehydrogenation of liquid hydrogen carriers, which to our knowledge has not been previously reported.

In this contribution, we show that highly active and stable dehydrogenation catalysts are prepared by solvent-free high energy ball milling by mixing only titania support and metallic platinum. The performance of the catalysts is studied in continuous gas-phase dehydrogenation of methylcyclohexane and compared with conventional incipient wetness impregnated catalyst. Extensive catalyst characterisation is carried out to elucidate the effect of the synthesis method on the catalyst properties, activity and stability.

2 Methods

2.1 Catalyst synthesis

2.1.1 Ball milling. All preparations were carried out using a Fritsch planetary micro mill P7 Pulverisette (classic line). The milling equipment included two custom-made corundum milling jars (45 ml each) and 10 mm ∅ corundum grinding balls (20 g in total for 10 balls per jar). Every time, the milling program comprised 15 min milling stages alternated with 5 min breaks. The two steps were repeated cyclically until the target milling time was finally accumulated. Rotation was inverted after each cycle to improve the homogeneity of the treatment. Typically, the milled powders were recovered in nearly

4144 | *Catal. Sci. Technol.*, 2025, **15**, 4143–4155

This journal is © The Royal Society of Chemistry 2025

quantitative yield by scraping the material with a spatula. Each preparation was repeated multiple times to ensure reproducibility.

The catalyst solid precursors, including the metallic Pt (325 mesh, ≥99.9%, Thermo Scientific) and oxide support (TiO$_2$ anatase, Sigma-Aldrich, 99.7%) powders, were loaded in the milling jar starting with the precursor with the highest loading mass, *i.e.*, support material. Every time, Pt loading of 1 wt% and preparation scale of 1 g was targeted. The solid mixture was milled for 3 h at 600 rpm. The ball milling parameters were selected based on our previous expertise on noble metal deposition on an oxide carrier with this mill geometry.[13] Furthermore, a time series of samples milled for 1, 3 and 6 hours was prepared and screened with XRD (not shown). The XRD patterns showed no significant difference in titania peaks between the samples milled for 3 or 6 hours, which suggests that a steady state was reached already after 3 hours of milling. Several repetitions of the synthesis were necessary to ensure enough material was available for follow-up characterisation and catalysis testing. The catalyst synthesised by ball milling was denoted as BM Pt/TiO$_2$.

2.1.2 Incipient wetness impregnation. Aqueous solution of tetraammineplatinum(II)nitrate (Alfa Aesar, 99.99%) was impregnated by incipient wetness technique to TiO$_2$ (P25, Sigma-Aldrich, ≥99.5%). The targeted Pt loading was 1 wt%. Prior to the impregnation, TiO$_2$ was calcined in air at 500 °C for 3 h and dried at 130 °C for 1 h. The Pt-solution was dispersed to the TiO$_2$ powder, and the impregnation process was let to stabilise for 48 h. After the incipient wetness impregnation, the prepared catalyst was calcined in air with 8 °C min^{-1} oven heating ramp to 500 °C, where the catalyst was retained for 4 h.

purification) was fed by an isocratic pump to a line, which was heated to 150 °C in order to vaporise MCH. Furthermore, 50 ml min^{-1} NTP of nitrogen was co-fed by Bronkhorst EL-Flow mass flow controller to ensure steady MCH flow through the reactor. The reactor was a quartz glass tube (length 580 mm, id 15 mm) with a glass frit located halfway of the reactor length. The catalyst bed (height ~2 cm) comprised of 0.2 g of studied catalyst mixed with 2.5 g of quartz sand, and the catalyst bed rested on the glass frit. The catalyst bed temperature was adjusted to the desired value using 50 ml min^{-1} nitrogen flow prior to starting the MCH feed. The reactor was operated under atmospheric pressure. After the reactor, the heated line (150 °C) continued all the way to an online GC (Agilent 6890) equipped with both TCD and FID detectors to analyse the dehydrogenation products in gas phase. Prior to the online GC there was a bypass valve to a condenser and a liquid–gas separator container. The function of the bypass line was not for sample collection, but to simply release excess pressure.

2.2.2 GC analytics. The dehydrogenation products were analysed in the gas-phase by Agilent 6890 gas chromatograph. The GC contained both thermal conductivity and flame ionisation detectors (TCD, FID), of which the TCD was used to analyse nitrogen and hydrogen, and FID the hydrocarbon products. The GC was equipped with both Restek Carboxen-1000 packed precolumn (SS general configuration, 60/80 mesh, 2.5 m, ID 2.1 mm, OD 1/8 in), and Agilent DB-1 dimethylpolysiloxane capillary column (50 m, ID 0.32 mm, film thickness 0.52 μm). Further GC method details are presented in the ESI.†

2.2.3 Result calculation. MCH conversion was calculated according to eqn (1), where the flow rates were calculated based on calibration corrected GC areas.

$$\text{Conversion (\%)} = \frac{\text{MCH flow rate}_{\text{IN}}\left(\frac{\text{mol}}{\text{min}}\right) - \text{MCH flow rate}_{\text{OUT}}\left(\frac{\text{mol}}{\text{min}}\right)}{\text{MCH flow rate}_{\text{IN}}\left(\frac{\text{mol}}{\text{min}}\right)} \cdot 100\% \tag{1}$$

Finally, the catalyst was cooled to room temperature and crushed into a fine powder with a mortar. The catalyst synthetized by the IWI technique was denoted as IWI Pt/TiO$_2$.

Toluene selectivity was calculated according to eqn (2), where the flow rates were calculated based on calibration corrected GC areas. The minor hydrocarbon side product (cyclohexane, benzene *etc.*) selectivity was calculated correspondingly.

$$\text{Selectivity (\%)} = \frac{\text{toluene flow rate}_{\text{OUT}}\left(\frac{\text{mol}}{\text{min}}\right)}{\text{MCH flow rate}_{\text{IN}}\left(\frac{\text{mol}}{\text{min}}\right) - \text{MCH flow rate}_{\text{OUT}}\left(\frac{\text{mol}}{\text{min}}\right)} \cdot 100\% \tag{2}$$

2.2 MCH dehydrogenation experiments

2.2.1 Reactor set-up. Gas-phase dehydrogenation of MCH was conducted in a continuously operated packed bed reactor, where the catalyst was always reduced online prior to the dehydrogenation experiments (H$_2$ feed rate 50 ml min^{-1} NTP for 2 h at 350 °C reactor temperature). The reactor set-up schematic is presented in Fig. S1.† Liquid methylcyclohexane (Sigma-Aldrich, 99%, used without further

Hydrogen production rate (eqn (3)) was calculated based on the molar flow of toluene by multiplying it with a factor of three, as three moles of H$_2$ are released of one mole of MCH during dehydrogenation to toluene. Furthermore, the amount of H$_2$ was confirmed with the GC, that was calibrated with known H$_2$ and N$_2$ feed rates. During the dehydrogenation experiments, the N$_2$ feed rate was always known, thus by assuming the N$_2$ feed rate in to be equal to N$_2$ flow out, the H$_2$ flow out could be

resolved. In eqn (3), Pt loading is the ICP-OES determined weight fraction of platinum in the catalyst mass.

$$\text{H}_2 \text{ production rate } \left(\frac{\text{mmol}_{\text{H}_2}}{\text{g}_{\text{Pt}} \text{ min}} \right) = \frac{\text{toluene flow rate}_{\text{OUT}} \left(\frac{\text{mmol}}{\text{min}} \right) \cdot 3}{(\text{catalyst mass (g)} \cdot \text{Pt loading})} \quad (3)$$

2.3 Catalyst characterisation techniques

2.3.1 N$_2$ sorption. The specific surface area (S_{BET}) of the fresh catalysts was measured using Micromeritics ASAP 2020. Nitrogen (-196 °C) was used as the adsorptive gas, and the specific surface area was calculated using the Brunauer–Emmett–Teller method. The samples were pretreated in vacuum in two steps: 30 minutes at 150 °C followed by 240 minutes at 150 °C to remove any physisorbed impurity compounds before the S_{BET} determination. The standard procedure was used for S_{BET} determinations using data points between 0.05 and 0.2 p/p_0.

2.3.2 ICP-OES. Metal content of the catalysts was determined with inductively coupled plasma optical emission spectroscopy (ICP-OES, 5110 SVDV, Agilent Technologies). The solids were first treated in microwave (Ethos Up, Milestone) by acid-assisted digestion method with different acid ratios (HNO$_3$, HCl and HF) and temperatures (220 and 230 °C). The digestion resulted clear solutions. The elements were analysed from 1/100 and 1/10 diluted samples. Multi elemental standard solutions provided by Inorganic Ventures and Merck were used as calibration standards and control samples in the ICP-OES measurement.

2.3.3 CO chemisorption and NH$_3$-TPD. Pt dispersion of the catalysts was assessed by static CO chemisorption, and their acidity was probed by NH$_3$ temperature programmed desorption. Both measurements were performed with Micromeritics 3Flex adsorption analyser. Detailed descriptions of the measurements are provided in the ESI.† Before the CO chemisorption, the catalyst samples were pre-treated by 1 h H$_2$ reduction at 350 °C. The CO chemisorption isotherms were measured at 35 °C. For the NH$_3$-TPD, the catalyst samples were pre-treated by He flush at 650 °C before adsorption of 5% NH$_3$ in helium at 50 °C. The temperature programmed desorption heating ramp was 10 °C min^{-1} to 650 °C.

2.3.4 TEM/EDS and HAADF-STEM. The catalysts were characterised using transmission electron microscopy and energy dispersive X-ray spectroscopy (TEM/EDS) at the Centre for Materials Analysis of the University of Oulu using the JEOL JEM-2200FS EFTEM/STEM. The dimensions of Pt particles were determined through analysis of HAADF-STEM images. A total of 140 to 170 Pt particles were considered for the calculation of particle size distribution by ImageJ software. The mean particle size of the support particles was deduced from 50 to 70 titania particles discerned in HR-TEM images. The presence and distribution of the metals was investigated with energy-dispersive X-ray spectroscopy (EDS) analysis.

2.3.5 SXRD/PDF. High-resolution synchrotron X-ray diffraction (SXRD) and total scattering methods were used to determine the phases present in the samples. All data was collected on the Brockhouse High Energy Wiggler beamline at the Canadian Light Source (CLS), Canada.[16] Data was collected in transmission mode using a 2D Perkin Elmer (Varex) detector (200 × 200 μm pixel size and 40 × 40 cm^2 area) at room temperature with powder samples loaded in Kapton capillaries with inner diameters of 0.81 mm. For SXRD a wavelength of 0.4087 Å (30.34 keV) was used with a sample to detector distance of 478.8 mm while for total scattering measurements the wavelength was 0.1905 Å (65.08 keV) with a distance of 134.8 mm. Ni was used as the calibrant. For the total scattering measurements empty Kapton capillaries were also measured under identical conditions to subtract the non-sample scattering. The 2D data were radially integrated into 1D diffraction patterns using the GSAS-II software.[17] To generate the pair distribution functions (PDFs), $G(r)$, a Q_{max} of 26 Å^{-1} was used.

2.3.6 XPS. Both *ex situ* standard XPS as well as *in situ* ambient pressure XPS (APXPS) were carried out for chemical characterisation of the catalyst. The *ex situ* XPS data on the catalysts was collected using a Thermo Fisher Scientific ESCALAB 250Xi XPS setup at the Centre for Materials Analysis of University of Oulu. ESCALAB 250Xi is equipped with a monochromatic Al anode X-ray source. For each catalyst a survey spectrum was recorded (binding energy range) for elemental composition analysis. High resolution XPS spectra were then collected for selected core levels (Pt 4f, C 1s, O 1s, Ti 2p) based on elements present in the samples. The spectra were collected for both as-synthesised and spent catalysts.

The *in situ* ambient pressure X-ray photoelectron spectroscopy (APXPS) measurements were performed at the HIPPIE beamline at the MAX IV Laboratory in Sweden.[18] The Pt 4f and Ti 3s spectra were recorded using photon energies of 1200 eV. Prior to the operando measurements, the catalyst was suspended in water and drop-cast onto a Si foil. The spectra were initially recorded for the as-synthesised catalyst. Subsequently, the catalyst was reduced under 1 bar of pure H$_2$ at 350 °C. Finally, the APXPS spectra were measured at 2 mbar MCH pressure and 345 °C and 365 °C. The Pt 4f and Ti 3s spectra were fitted using a Tougaard background with DS line shapes.

2.3.7 Raman & carbon content. Raman measurements were done using Timegated® Pico Raman spectrometer with a pulsed excitation laser (532 nm) and a time-resolved single-photon counting detector to find out the carbonaceous compounds on the surface. The spectra were collected at the Raman shift range from 100 to 2000 cm^{-1} with spectral resolution of ~4 cm^{-1} at room temperature and ambient atmosphere. The samples contained catalyst and quartz sand

4146 | *Catal. Sci. Technol.*, 2025, **15**, 4143–4155

This journal is © The Royal Society of Chemistry 2025

in a ratio of 1:12.5. The carbon content of the fresh and spent catalysts was analysed by Leco CS230 analyser.

3 Results & discussion

3.1 Catalyst synthesis and physical properties

Titania-supported platinum catalyst was synthesised by both ball milling and incipient wetness impregnation methods, denoted BM and IWI, respectively. The ball-milled catalyst was prepared by simply milling metallic Pt powder with anatase-phase titania in a planetary ball mill equipped with corundum grinding balls and jars. The program was selected based on our earlier studies, which showed that 3 h was sufficient to disperse the metal on the support surface.[13] Furthermore, we expected the high-energy milling to transform the anatase into rutile. Several batches of 1 g scale were made and combined to improve reproducibility.

Incipient wetness impregnation method was applied to prepare a more conventional catalyst as a point of reference. To align with the majority of catalysts studied in the scientific works, we selected a commonly used commercial titania P25 support, which is a mixture of anatase and rutile. Based on a previous report, this type of support outperformed pure anatase support in LOHC dehydrogenation.[9] According to BET analysis, both catalysts had a specific surface area in similar range, around 50 $m^2 g^{-1}$ (Table 1). The adsorption average pore width by BET analysis was 6 nm for the BM catalyst, and slightly larger 9 nm for the IWI catalyst. Analysis of the metal content by ICP showed that BM Pt/TiO_2 contained 0.92 wt% Pt, whereas IWI Pt/TiO_2 had a lower Pt content of 0.83 wt%. The nominal concentration was 1 wt% for both catalysts, indicating that the metal is loaded more efficiently using the mechanochemical synthesis compared to IWI, which is beneficial from both economic and environmental aspects.

3.2 MCH dehydrogenation experiments

The dehydrogenation of vaporised MCH was carried out in a continuous flow reactor at atmospheric pressure. Liquid MCH was pumped to a heated (150 °C) process line together with nitrogen to facilitate a steady reactant flow through the reactor. The catalyst bed comprised of catalyst powder mixed with quartz sand, and the catalyst was reduced *in situ* prior to the MCH dehydrogenation. The reaction products were analysed online by gas chromatography. A more detailed process scheme is provided in the experimental section of this paper.

Before experimenting with the catalysts, we wanted to have an understanding on the effect of the reaction parameters on

MCH conversion and stability using the conventional impregnated catalyst IWI Pt/TiO_2. A simple experimental design matrix was used to find the optimal conditions over 0.2 g of IWI Pt/TiO_2. The studied factors were the MCH feed rate (0.1–0.2 ml min^{-1}) and temperature (300–350 °C), while other reaction conditions were maintained constant (see ESI† Section S2.1). The minimum value for MCH feed rate was the minimum flow rate of the liquid feeding pump, and the maximum was double the minimum. MCH was co-fed with 50 ml min^{-1} of N_2 to ensure steady gas flow. The minimum temperature 300 °C was chosen based on literature,[7] which suggested that lowering the temperature might be beneficial to decrease coke formation and thus inhibit the catalyst deactivation. The maximum temperature 350 °C was the typical MCH dehydrogenation temperature seen in relevant literature.[3,7] The reaction parameters were chosen with emphasis on highlighting the possible differences between the two catalysts instead of solely maximising the MCH conversion.

All the MCH dehydrogenation condition screening experiments had a high selectivity to toluene (>99.5%), hence our emphasis on analysis focuses on catalyst activity which was more responsive to the varied process conditions. During the first hour of the experiment, the conversion of MCH was between 20–70% depending on the conditions (Fig. S2†). However, the conversion showed a slight decline over time on stream, which prompted us to calculate the rate of deactivation for the reaction as decrease of the MCH conversion per hour. Interestingly, the rate of deactivation varied depending on the reaction conditions. Based on these observations, we used the conversion and H_2 productivity at 4 h along with the rate of deactivation as responses for the statistical analysis (Table S1†). The results were fitted using MODDE software version 13.0.2 (see ESI† for detailed information). Temperature had the biggest positive influence on both conversion and H_2 production (Fig. S3 and S4†). However, increasing the temperature also increased the deactivation rate. While increasing the feed rate had a slightly positive effect on H_2 production, it also caused increased deactivation and decreased conversion. Based on the analysis, we chose to use 345 °C and MCH feed rate 0.1 ml min^{-1} for catalyst comparison studies. At lower temperatures (300–325 °C), the H_2 productivity was insufficient, whereas the higher MCH feed rate (0.2 ml min^{-1}) caused rapid catalyst deactivation.

Next, we wanted to compare the ball milled and impregnated Pt/TiO_2 catalysts at the chosen conditions (345 °C, 0.1 ml min^{-1} MCH feed rate, 0.2 g catalyst). The experiments were operated for 15 h, or until the catalyst fully deactivated. The MCH conversion of IWI Pt/TiO_2 started at around 70% and decreased to around 45% during the 15 h TOS (Fig. 1). The initial MCH conversion of BM Pt/TiO_2 was around 50%, thus lower than for its IWI prepared counterpart. However, the deactivation rate of BM Pt/TiO_2 was lower than that of the IWI catalyst, and the MCH conversion of BM Pt/TiO_2 was around 40% at the end of the experiment (Table S2†). In addition to the experiments

Table 1 Characterisation results of the in-house synthesised catalysts

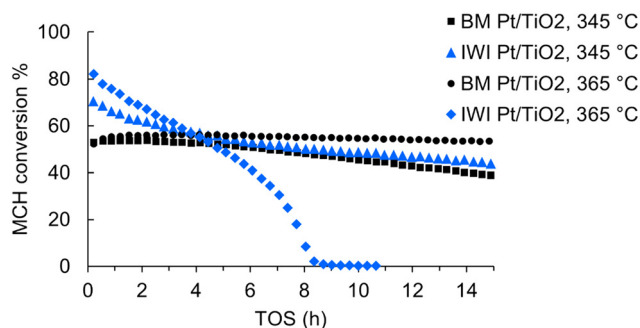| Catalyst	S_{BET} ($m^2 g^{-1}$)	Pore size (nm)	Pt content (wt%)
BM Pt/TiO_2	54	6.1	0.92
IWI Pt/TiO_2	50	9.0	0.83

Fig. 1 Catalytic performance of the monometallic Pt/TiO$_2$ catalysts in terms of MCH conversion at two different temperatures: 345 and 365 °C. Atmospheric pressure, 0.2 g catalyst, MCH feed rate 0.1 ml min^{-1}.

performed at 345 °C, we tested the catalysts at a higher temperature of 365 °C in 15 h experiments (Fig. 1). In these conditions, the IWI Pt/TiO$_2$ catalyst completely deactivated in just 9 hours on stream, supporting the observation of the effect of temperature on the deactivation. Remarkably, the ball-milled catalyst showed different behaviour; the increased temperature stabilised the BM Pt/TiO$_2$ catalyst, and the deactivation rate during the 15 h experiment was only 0.2 Δmol% h^{-1}. The MCH conversion remained constant at around 55%. At 15 h TOS, the hydrogen production rate was 670 mmol$_{H_2}$ g$_{Pt}^{-1}$ min^{-1}, which is among the highest reported (Table S3†). To our knowledge, higher rates in MCH dehydrogenation have only been observed with a trimetallic Pt$_3$(Fe$_{0.75}$Zn$_{0.25}$)/SiO$_2$ catalyst[19] and a single atom Pt$_1$/CeO$_2$,[20] 757 and 2509 mmol$_{H_2}$ g$_{Pt}^{-1}$ min^{-1}, respectively.

Analysis of side products in the outlet gas showed that all of the aforementioned experiments had over 99% selectivity to toluene (Fig. S5†). Minor amounts of hydrocarbon side products, which were attributed to partially dehydrogenated intermediate products such as methylcyclohexene, were observed (Fig. S6†). Selectivity to demethylation products *i.e.*, cyclohexane and benzene, varied between 0–0.12% (Fig. S7†). Methane concentrations were measured in the process gas arriving to the online GC (Fig. S5†). No CO or CO$_2$ were observed above the detection limit, which for the TCD-GC setup was about 1000 ppm. The highest amount of side products was detected with IWI Pt/TiO$_2$ at 365 °C; over 1.2% selectivity to hydrocarbon side products and over 50 ppm methane were observed just before the catalyst deactivated. At 345 °C, IWI Pt/TiO$_2$ produced about 20 ppm methane and the side product selectivity was about 0.4%. Remarkably, in case of BM Pt/TiO$_2$, the selectivity to side products decreased from 0.3% to less than 0.2% upon increasing the temperature from 345 to 365 °C and furthermore, no cyclohexane or benzene were detected at 365 °C. It is also important to point out that we could not detect any methane in the experiments with the ball-milled catalyst, which highlights its superior stability and selectivity in MCH dehydrogenation.

In industrial Pt-catalysed processes for hydrocarbons, such as naphtha reforming, a small co-feed of hydrogen is often used to maintain optimal hydrogen pressure and prevent coking.[21–23] In our experiments, we chose to study the catalysts without additional hydrogen. Firstly, it allowed to better observe the differences in catalyst activity and deactivation, and secondly, it would be ideal to develop a robust catalyst and omit the need for additional hydrogen. To study if the additional hydrogen stabilises the conversion as efficiently as the temperature elevation to 365 °C, we performed an experiment with a small additional 5 ml min^{-1} hydrogen feed for BM Pt/TiO$_2$ at 345 °C (Fig. S8†). While the co-fed H$_2$ helped to decrease the catalyst deactivation, increasing the temperature had a more pronounced effect on stability for the BM Pt/TiO$_2$ catalyst. Furthermore, the conversion at 15 h TOS was about 45% in the H$_2$ co-feed experiment at 345 °C, and about 55% in the 365 °C experiment.

3.3 Catalyst characterisation

To better understand the properties and activity of the catalysts, detailed characterisation was carried out for the fresh catalysts before reduction. The spent catalysts were recovered from the reactor as a mixture with quartz sand and the mixture was analysed to investigate the catalyst deactivation.

3.3.1 SXRD/PDF. The crystalline phases of the fresh catalysts were investigated by SXRD as presented in Fig. 2. The patterns of BM Pt/TiO$_2$ correspond mainly to tetragonal rutile phase (PDF 00-021-1276). While the support material used for the ball milled catalyst synthesis was anatase, phase transformation of anatase to more stable rutile occurred during ball milling. Only traces of anatase were left after milling, as evidenced by the weak hump at $2\theta = 6.66°$ that can be assigned to the (101) diffraction peak from anatase phase in the ball milled patterns. The phase transformation has previously been reported in several studies, including our previous work.[13] While the exact mechanism is still unknown, it has been suggested that the phase transformation is induced by the high local temperatures and pressures at the point of contact of the colliding balls with the powder and vessel.[10] In a recent study, Mechiche *et al.* show that phase transformation of alumina can be rationalised by two key parameters, the shock energy and the number of shocks.[24]

The impregnated IWI Pt/TiO$_2$ showed patterns corresponding to a mixture of rutile and anatase (PDF 00-021-1272) with a ratio around 1:9, consistent with earlier reports.[9] Pt-related diffraction peaks were only observed in the pattern for IWI Pt/TiO$_2$ in Fig. 2b, while no such features were seen in other patterns due to the low noble metal content and small particle size.

A closer look at the diffraction patterns reveals that the rutile peaks of the ball-milled samples are broader than the anatase peaks in the impregnated samples, indicating smaller crystallite size or higher disorder of the support in the ball-milled catalysts. Mean crystallite sizes of the support for ball-milled catalysts estimated by Scherrer equation from
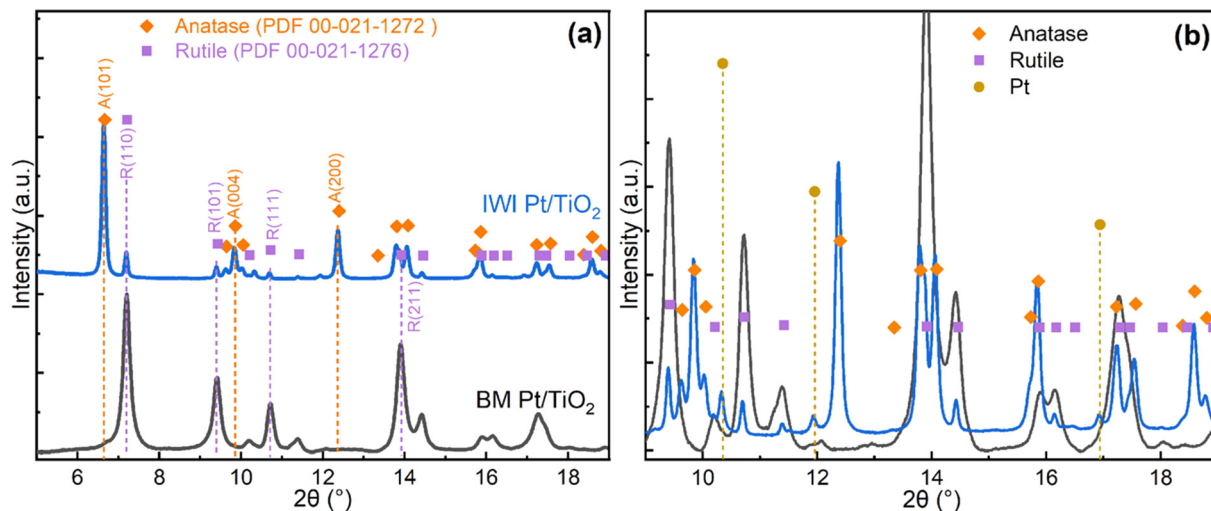
Fig. 2 (a) Synchrotron X-ray diffraction profiles and (b) magnified view of the catalyst samples.

the rutile (110) reflection are about 20 nm. The structural order of the catalysts is also evident from the PDF profiles, which show peaks characteristic to the corresponding titania phases (Fig. S9†).

3.3.2 Particle size analysis

Fresh catalysts. The nano-to-micro-scale morphology and particle size distribution of the catalysts was investigated with transmission electron microscopy (TEM) and high-angle annular dark-field scanning transmission electron microscopy (HAADF-STEM). The predominant size distribution of titania particles in all samples was concentrated within the range of 10 to 20 nm (Fig. S10†). The average size of the metal particles was determined from the fresh catalysts prior to reduction. In case of BM Pt/TiO$_2$, the Pt particles were uniformly distributed across the titania particles, and the mean Pt particle size was 0.7 nm with a rather large standard deviation at 0.5 nm (Fig. 3a and c, Table S4†). Some larger Pt particles over 10 nm were also observable, however, these were excluded from the particle size calculations due to their minor representation in comparison to the smaller particles. EDS analysis confirms the even distribution of Pt on the support (Fig. S11†).

In case of IWI Pt/TiO$_2$, the Pt particle size varied between 0.6 nm to 2.0 nm with an average of 1.3 nm (Fig. 3d). The Pt particles were non-uniformly distributed on the support, with Pt being selectively present on specific TiO$_2$ particles (Fig. 3b and S11†). Similar observation was reported by Iddir *et al.* when investigating Pt deposition on P25 titania; Pt particles preferred nucleation on rutile particles rather than anatase particles, which was attributed to the higher number of oxygen vacancies in the rutile phase.[25] Compared to its ball-milled counterpart, the impregnated catalyst clearly showed wider particle size distribution and larger average particle size.

Pt dispersion of the catalysts was measured by static CO chemisorption (ESI† Section S3.7). Prior to the measurement, the catalysts were reduced with H$_2$ at 350 °C, similarly to the reduction before the dehydrogenation experiments. Interestingly, the BM Pt/TiO$_2$ catalyst showed only 8.3%

dispersion and IWI Pt/TiO$_2$ 12.1% dispersion. These values are significantly lower than what can be calculated based on geometry[26] and the mean particle size determined by TEM; the IWI catalyst Pt dispersion should be 86% whereas the BM catalyst should have nearly full dispersion. Platinum is known to have strong metal-support interactions (SMSI) with some support materials, for instance titania, which result in encapsulation of the metal particles with a thin layer of the support material and thus reduced chemisorption of CO.[27]

Spent catalysts. To investigate the changes caused by the MCH dehydrogenation, the catalyst particle size and distribution were characterised after the experiments at 345
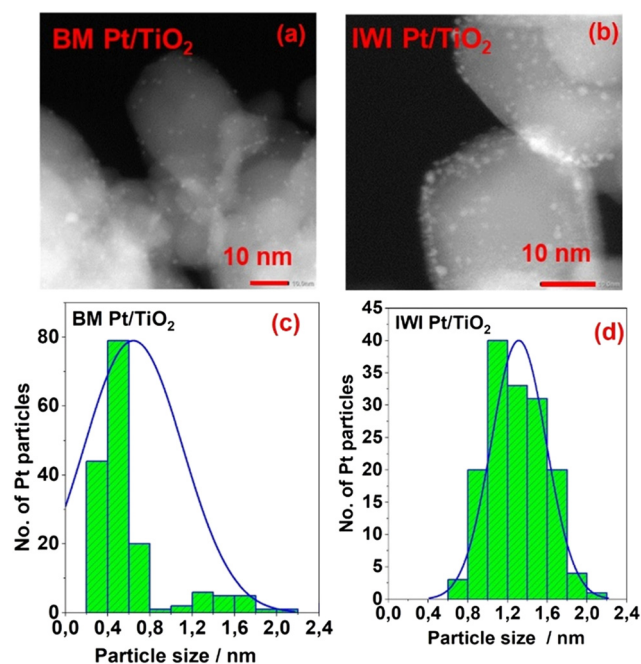

Fig. 3 HAADF-STEM images and Pt particle size distributions of the fresh catalysts (a and c) BM Pt/TiO$_2$, (b and d) IWI Pt/TiO$_2$.

This journal is © The Royal Society of Chemistry 2025

Catal. Sci. Technol., 2025, **15**, 4143–4155 | **4149**

Table 2 Mean Pt particle size of fresh and spent catalysts according to TEM

Catalyst	Average Pt metal particle size and standard deviation (nm)		
	Fresh	Spent at 345 °C	Spent at 365 °C
BM Pt/TiO$_2$	0.7 ± 0.5	1.0 ± 0.5	1.1 ± 0.3
IWI Pt/TiO$_2$	1.3 ± 0.2	1.3 ± 0.3	1.7 ± 0.3

°C and 365 °C (Fig. S12 and S13†). After the dehydrogenation at 345 °C, the BM Pt/TiO$_2$ showed a slight increase in the Pt particle size from 0.7 nm to 1.0 nm (Table 2). Increase to 365 °C did not inflict further growth of the metal particles, highlighting the stability of the ball-milled catalyst. Ball milling is known to increase surface defects,[10] which has been shown to improve anchoring of nanoparticles to increase the stability.[28] In case of IWI Pt/TiO$_2$, the Pt particle size of the catalyst spent at 345 °C was similar to the fresh catalyst, around 1.3 nm. However, at 365 °C the Pt particle size increased slightly from 1.3 nm to 1.7 nm.

3.3.3 XPS. The composition and state of the elements on the catalyst surface was studied by X-ray photoelectron spectroscopy (XPS) using lab based UHV XPS for the fresh and spent catalysts. Furthermore, *in situ* XPS measurements were carried out using APXPS to investigate the changes during the dehydrogenation experiments.

Fresh catalysts. The XPS measured Pt 4f and Ti 3s spectra of fresh catalysts prior to reduction are presented in Fig. 4. In all the catalysts, the Ti 3s peak was observed at 62.6 eV with two charge transfer satellite peaks at 66.4 and 75.8 eV (red in Fig. 4).[29] The BM Pt/TiO$_2$ catalyst exhibited a complex mixture of various Pt oxidation states based on the Pt 4f peak; metallic Pt^0 (71.1 eV, blue color),[30] Pt^{2+} (73 eV, navy blue color) and Pt^{4+} (75.1 eV, green).[31] Another peak was observed centred at 72 eV (dark yellow), between the levels of Pt^0 and Pt^{2+}, indicating a partial positive charge of Pt. This peak is assigned as Pt$_n$ in the figures. Based on quantification of the Pt peak areas, this was the most abundant Pt species in the BM Pt/TiO$_2$ catalyst (Fig. S14a†).

Potentially, this peak could originate from the very small Pt particles, as similar positive shifts of about 1 eV have been reported previously for single atom Pt catalysts.[32,33] Another possibility is interaction with titania; Pt is known to form SMSI with titania, which can result in an overlayer of titania on the metal partiles.[5] Beck *et al.* assigned a similar peak to Pt–O at the interface of the titania overlayer.[34] The observation of SMSI is supported by the chemisorption results which indicate partial encapsulation or coverage of Pt with titania. Furthermore, an additional peak at 460.1 eV was observed in the Ti 2p spectrum, which could originate from charge transfer between the support and Pt (Fig. S15†).[32,35,36]

The fresh IWI Pt/TiO$_2$ catalyst contained mostly platinum in oxide states Pt^{4+} and Pt^{2+}, and only a small amount of Pt^0 was detected (Fig. 4b). This was expected since no reductive treatment was made during the catalyst preparation. Curiously, no Pt peak at 72 eV was observed in the impregnated sample.

Spent catalysts. To investigate changes in the oxidation states, we analysed the catalysts (as a mixture with quartz sand) after the dehydrogenation experiments. Fig. 5 depicts the Pt 4f spectra of the catalysts used at 345 °C and 365 °C, as denoted in the figures. The relative percentages of the Pt species are presented in Fig. S14b.† In all samples, most of Pt was present as metallic Pt^0, discerned by a characteristic peak at 70.9 eV. This is expected after reducing the catalysts with H$_2$ prior to the dehydrogenation experiments. Nevertheless, a noticeable presence of Pt$_n$ species at 72.2 eV was observed in the spent BM Pt/TiO$_2$ catalysts (Fig. 5a and c). The relative amount of Pt$_n$ increased with increasing the reaction temperature (Fig. S14b†). This indicates that the Pt$_n$ peak arises from the SMSI and interaction with titania; the titania overlayer is known to grow during prolonged times at increased temperatures.[34] Additionally, a minor peak corresponding to Pt^{4+} at 75 eV was observed in the BM Pt/TiO$_2$ 365 °C sample. In case of IWI Pt/TiO$_2$ catalyst, a new peak at 72.1 eV was detected in the spent IWI Pt/TiO$_2$ catalyst at 365 °C. This peak is assigned to PtO$_x$ species in Fig. 5. The PtO$_x$ species is likely attributed to partial oxidation of the spent catalyst, caused by prolonged air
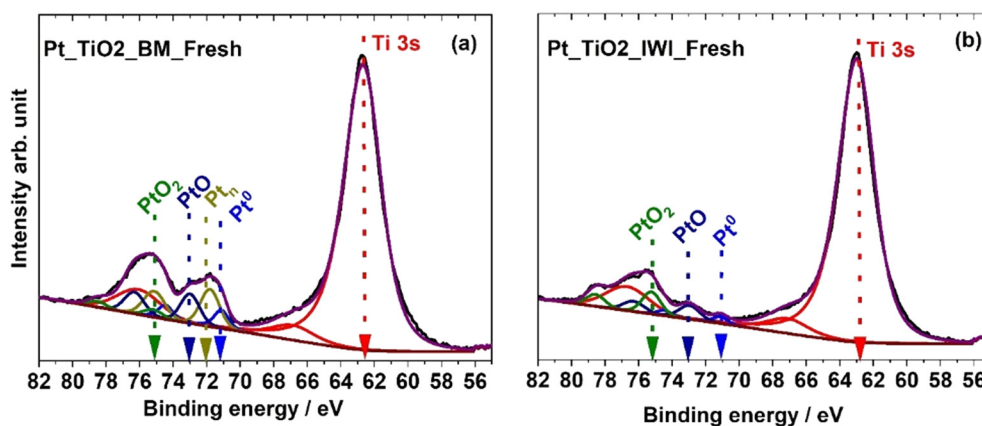

Fig. 4 Pt 4f and Ti 3s spectra for fresh catalyst. (a) BM Pt/TiO$_2$ and (b) IWI Pt/TiO$_2$.
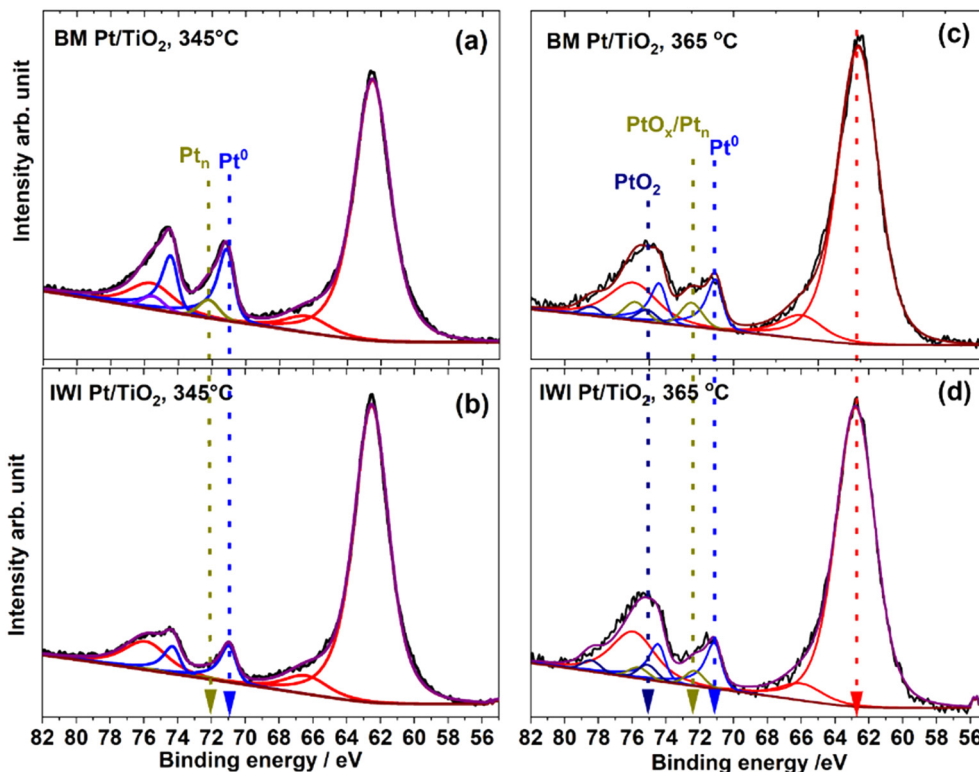
4150 | *Catal. Sci. Technol.*, 2025, **15**, 4143–4155

This journal is © The Royal Society of Chemistry 2025

Fig. 5 The Pt 4f and Ti 3s spectra of spent catalysts after dehydrogenation at different temperatures. (a) BM Pt/TiO$_2$, 345 °C (b) IWI Pt/TiO$_2$, 345 °C (c) BM Pt/TiO$_2$, 365 °C and (d) IWI Pt/TiO$_2$, 365 °C.

exposure between the MCH dehydrogenation reaction and the UHV XPS measurements. As explained *vide infra*, this species was not observed in the APXPS measurements. No significant changes were observed in the Ti 3s spectra compared to the fresh catalyst XPS spectra (not shown).

Ambient pressure XPS (APXPS). To further investigate the changes in the electronic structure of the catalysts during the experiments, APXPS measurements were carried out at HIPPIE beamline at MAX IV, which enabled *in situ* reduction and MCH dehydrogenation during the XPS measurement. The Pt 4f and Ti 3s spectra of BM and IWI Pt/TiO$_2$ were initially recorded for the fresh catalyst and, subsequently, after the catalyst was reduced under 1 bar of pure H$_2$ at 350 °C. Finally, the APXPS spectra were measured at 2 mbar MCH pressure at 345 °C (Fig. 6) and 365 °C (Fig. S16†).

The spectra of the fresh catalysts are very similar to those recorded with UHV XPS (Fig. 4 *vs.* 6). The ball-milled catalyst contained metallic Pt, various Pt oxides, including Pt^{2+} and Pt^{4+}, and the Pt$_n$ peak at 72 eV attributed to the SMSI and interaction with titania. The spectra of the IWI catalyst also closely resemble those described in the UHV XPS analysis. The Ti 3s spectra are consistent with those observed in UHV measurements, with binding energies similar to those found in UHV XPS.

After reduction of the catalysts at 350 °C, Pt is reduced to Pt^0 in both catalysts. However, in the ball-milled catalyst, a partial positive charge on Pt (Pt$_n$), is still observable, indicating more pronounced SMSI in the ball-milled catalyst.

In contrast, all Pt oxides are fully reduced to Pt^0 in the IWI catalyst. Additionally, Ti is partially reduced to TiO$_x$, as indicated by the orange peak fitted at 60 eV.[27] The detection of reduced Ti species in both catalysts, likely arising from high-temperature treatment under H$_2$ atmosphere, is indicative of partial TiO$_2$ reduction. Separately, the observed Pt$_n$ peak as well as the decrease in Pt dispersion, as measured by CO chemisorption, is consistent with the manifestation of strong metal–support interactions (SMSI), in agreement with previous reports on Pt/TiO$_2$ systems.

The *in situ* APXPS observations highlight that the chemical state of Pt during the dehydrogenation is very similar to that of the reduced and spent catalysts, indicating that there is no transient state of the catalyst under MCH exposure. The catalysts were tested for more than 3 hours under operando conditions at 345 °C (Fig. 6) and 365 °C (Fig. S16†), showing no significant changes over time. Both catalysts exhibit rather similar characteristics, indicating comparable surface chemistry and electronic environments of Pt and TiO$_2$ at these temperatures. In both catalysts, Pt^0 is the predominant species during the MCH dehydrogenation. Interestingly, the Pt$_n$ peak is present in the BM Pt/TiO$_2$ during the dehydrogenation, which corroborates the SMSI in the ball mill-prepared catalyst. In case of IWI Pt/TiO$_2$, only Pt^0 species was observed, which suggests that the PtO$_x$ peak observed in the UHV XPS measurements of the spent catalyst is likely due to partial oxidation caused by prolonged air exposure between the dehydrogenation experiment and the XPS analysis. This underscores the
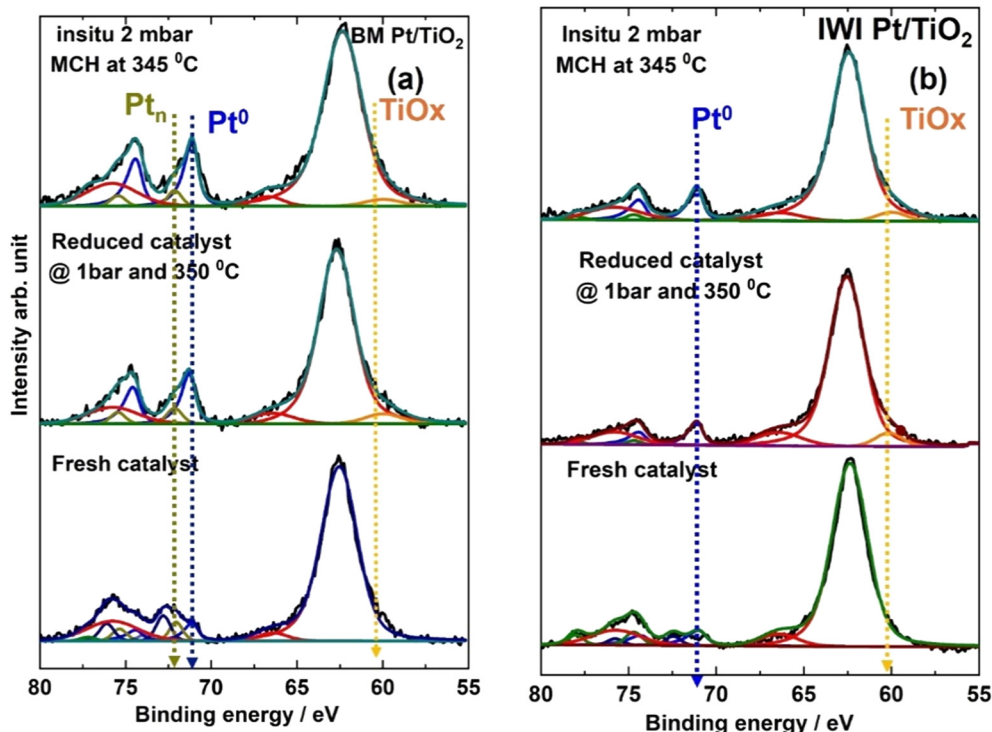
This journal is © The Royal Society of Chemistry 2025

Catal. Sci. Technol., 2025, **15**, 4143–4155 | **4151**

Fig. 6 APXPS Pt 4f and Ti 3s spectra recorded for fresh catalyst (bottom), after reduction (middle) and during the dehydrogenation (top) for (a) BM Pt/TiO$_2$ and (b) IWI Pt/TiO$_2$.

importance of performing *in situ* XPS analyses to accurately capture the true oxidation states of active species during catalytic reactions, as *ex situ* measurements can be misleading due to post-reaction changes.

3.3.4 Deactivation studies. The characterisation of the spent catalysts by TEM and XPS showed no dramatic changes in particle size or electronic structures of the catalysts which could explain the different stabilities of the catalysts. To further elaborate the deactivation, we measured carbon content of the spent catalysts to quantify coke and coke precursors. The fresh catalysts were measured as baseline, and both contained less than 100 ppm carbon (Fig. 7). The catalysts used at 345 °C showed a somewhat higher carbon content, 160 ppm in BM Pt/TiO$_2$ and 200 ppm in IWI Pt/TiO$_2$. However, a considerable difference was observed in the

Fig. 7 Carbon content of the fresh and spent BM Pt/TiO$_2$ and IWI Pt/TiO$_2$ catalysts.

catalysts after the experiments at 365 °C; the ball-milled catalyst had 170 ppm carbon, while the impregnated catalyst contained over 800 ppm carbon. These results clearly indicate that the full deactivation of IWI Pt/TiO$_2$ at 365 °C was caused by coking. In contrast, the ball-milled catalyst showed remarkable resistance towards coking even at the elevated temperature.

The catalyst samples were further analysed by Raman spectroscopy to elaborate the carbonaceous compounds present. The fresh catalysts were measured as a mixture with quartz sand to enable comparison with the spent catalysts. The fresh BM and IWI catalysts had quite similar spectra in general (Fig. 8). The strong bands in the range from 100 to 800 cm^{-1} are mainly caused by titania support (marked as TiO$_2$ in the figure) and used quartz sand (marked as Q in the figure).[37,38] Characteristic sp^2 carbon bands and their composites determined in the spent samples are G band (1580 cm^{-1}) and D band (between 1300–1400 cm^{-1}).[39,40] These bands are negligible over the fresh catalyst samples. In the spent ball-milled catalyst samples, both the G and D bands are weakly visible in the BM Pt/TiO$_2$ 345 °C sample but not visible in BM Pt/TiO$_2$ 365 °C (Fig. 8a). Conversely, the spent IWI Pt/TiO$_2$ samples show much stronger carbon bands; a small increase can already be detected in IWI Pt/TiO$_2$ 345 °C, whereas the G band is clearly at its strongest in the IWI Pt/TiO$_2$ 365 °C sample. The results gained are well in line with the total carbon content measurements and confirm that the IWI Pt/TiO$_2$ catalyst was deactivated by carbonaceous compounds at 365 °C.
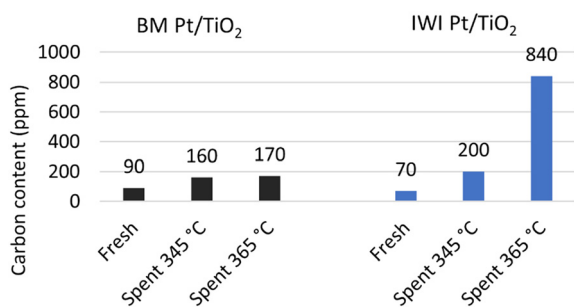
4152 | *Catal. Sci. Technol.*, 2025, **15**, 4143–4155

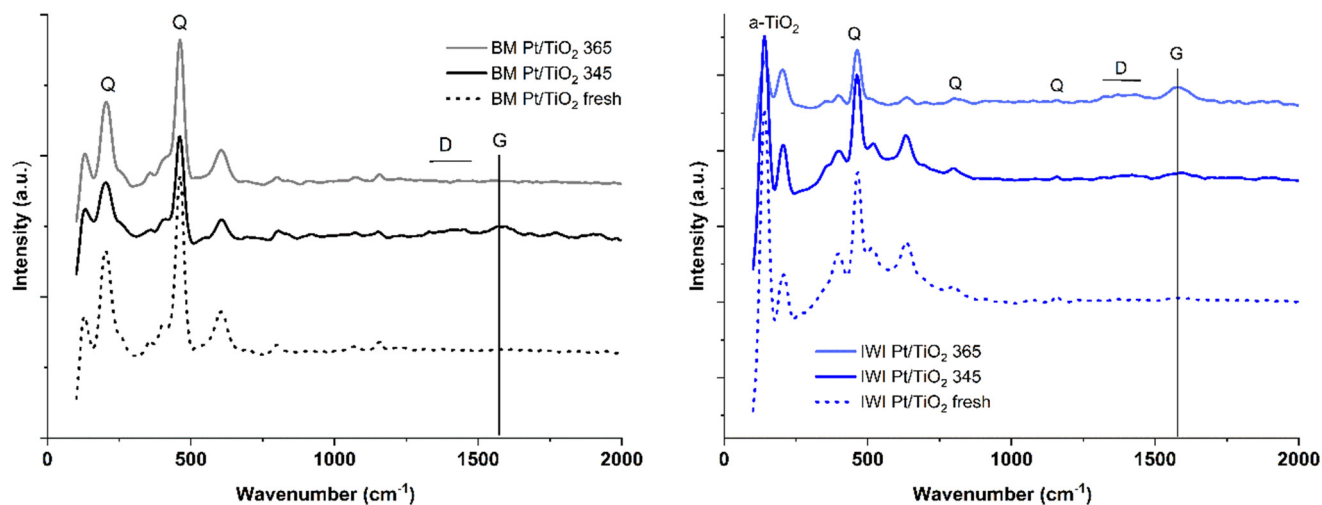This journal is © The Royal Society of Chemistry 2025

Fig. 8 Raman spectra of fresh and spent BM Pt/TiO$_2$ (left) and IWI Pt/TiO$_2$ (right) catalysts. D and G denote carbonaceous species, Q quartz.

The formation of graphitic carbon is further corroborated by the APXPS measurements. Fig. S17† illustrates the evolution of the C 1s spectra obtained during the *in situ* dehydrogenation of MCH. Two distinct C 1s peaks are observed in the spectra. The first peak, located at 284.4 ± 0.1 eV, is attributed to adventitious carbon,[41] while the second peak, positioned at 285.5 ± 0.1 eV, corresponds to gas-phase MCH carbon. These features are consistent for both the BM and IWI catalysts. Under reaction conditions of 2 mbar and elevated temperatures of 345 °C and 365 °C, the C 1s spectra for the BM catalyst remain unchanged relative to those recorded for the reduced catalyst. This suggests that the surface chemistry of the BM catalyst, with respect to carbon species, remains stable during MCH dehydrogenation, and no significant alteration in binding energy is observed. In contrast, the C 1s peak located at the 284.4 eV for the IWI catalyst exhibit a ~0.3 eV shift towards lower binding energies to 284 eV when compared to the spectra collected after the reduction process. The shift towards lower binding energy is commonly associated with the formation of graphitic carbon as the carbon atoms become more covalently bonded to the metal catalyst, leading to changes in their electronic environment.[42]

Previous studies have suggested that deactivation can be caused by adsorption of the produced toluene on the catalysts, which can lead to formation of coke.[5,21] A plausible reason for the different coking behaviour of the two catalysts might be their different acidity, which originates from the different titania polymorphs. Anatase is known to be more acidic than rutile, and the acidity of the support is known to increase coke formation.[7] To further investigate the catalysts, we measured the acidity by NH$_3$-TPD measurements (Fig. S19†). The quantity of NH$_3$ desorbed within the measured temperature range of 50–650 °C was 138 and 307 μmol g^{-1} for BM Pt/TiO$_2$ and IWI Pt/TiO$_2$, respectively. The result confirms that the anatase-supported IWI Pt/TiO$_2$ has in total over twice as many acid

sites as the rutile-supported BM Pt/TiO$_2$. Interestingly, BM Pt/TiO$_2$ had also a minor amount of strong acid sites (NH$_3$ desorption peak maximum at 500 °C)[43] that the IWI catalyst did not present. While NH$_3$-TPD does not separate Lewis acid sites from Brønsted acid sites, reports in the literature have shown that the acid sites on rutile are predominantly Lewis acid sites.[44] Brønsted acid sites can induce cracking reactions leading to unwanted products and further to catalyst coking.[45] Analysis of the side products of MCH dehydrogenation reveals that the formation of side products and especially methane increased prior to the deactivation of IWI Pt/TiO$_2$ at 365 °C (Fig. S5†). Remarkably, no methane was observed with BM Pt/TiO$_2$ and at 365 °C the catalyst produced no C6 side products resulting from cracking.

In addition to the support acidity, the catalysts differ in the electronic state of the Pt during the dehydrogenation. The partial positive charge of Pt$_n$, which arises from the SMSI, could facilitate the desorption of toluene from the Pt surface; DFT calculations by Tuo *et al.* showed that electron deficient state of Pt decreased the adsorption energy of the aromatic product leading to enhanced dehydrogenation activity.[46] As toluene adsorption on the catalyst has been shown to lead to coke formation,[5] the Pt$_n$ species observed on BM Pt/TiO$_2$ can play an important role in preventing the coking.

The combination of total carbon, APXPS and Raman results provides a robust confirmation of the IWI catalyst deactivation mechanism through the formation of carbonaceous compounds under the reaction conditions. The NH$_3$-TPD measurements confirm that the ball-milled catalyst benefits from a significantly lower acid site density compared to the IWI prepared catalyst. Furthermore, the SMSI on the BM catalyst facilitates desorption of the produced toluene from the platinum surface. These factors combined ensure the improved stability and resistance towards cracking reactions and coking.

4 Conclusions

Efficient and stable catalysts for the hydrogen release from liquid organic hydrogen carriers are crucially important for the feasibility of LOHCs in storage and transport of hydrogen. In this work, we have shown a waste-free mechanochemical synthesis to produce highly active and stable Pt catalysts for the dehydrogenation of methylcyclohexane into toluene. By mixing simply metallic platinum and anatase-phase titania powder in a high energy ball mill, stable nanometre-sized Pt particles were evenly distributed onto the titania support, and furthermore, phase transformation of anatase to rutile was observed.

Comparison of the ball-milled catalyst with a conventionally impregnated platinum catalyst in the dehydrogenation of methylcyclohexane clearly showed the high activity and superior stability of the mechanochemically prepared BM Pt/TiO$_2$ catalyst. The best performance was achieved at 365 °C; the BM Pt/TiO$_2$ catalyst was stable throughout the 15 h experiment. The hydrogen production rate was 670 mmol$_{H_2}$ g$_{Pt}^{-1}$ min^{-1}, which is among the highest values reported for methylcyclohexane dehydrogenation. At the same conditions, the conventionally impregnated IWI Pt/TiO$_2$ fully deactivated already at 9 h TOS due to coking. The ball-milled catalyst also showed higher selectivity towards toluene compared to the impregnated catalyst. Based on our characterisations, the rutile support of the BM Pt/TiO$_2$ catalyst is less acidic compared to the anatase-rich IWI Pt/TiO$_2$, which increases resistance towards coke formation. Furthermore, a partial positive charge on Pt, arising from interaction of the platinum with the support titania, facilitates the desorption of the produced toluene and prevents coking.

Data availability

The authors confirm that the data supporting the manuscript "Mechanochemical synthesis of Pt/TiO$_2$ for enhanced stability in dehydrogenation of methylcyclohexane" by Krista Kuutti *et al.* are available within the article and its ESI.†

Author contributions

KK: methodology, investigation, visualization and writing – original draft. MG: investigation, formal analysis, visualization and writing – review & editing. PP: conceptualization and methodology. JDB: methodology and investigation. PJ: methodology and investigation. HS: investigation, formal analysis and visualization. SW: investigation, formal analysis and visualization. GK: investigation. JFC: investigation. FS: methodology and resources. KA: investigation and analyses. MiH: investigation, analyses, funding acquisition and writing – review & editing. MaH: supervision, funding acquisition and resources. SU: conceptualization, investigation, formal analysis, supervision, project administration and writing – review & editing. SR: conceptualization, formal analysis, supervision, funding acquisition and writing – review & editing.

Conflicts of interest

The authors declare no conflicts of interest.

Acknowledgements

References

1 S. Atilhan, S. Park, M. M. El-Halwagi, M. Atilhan, M. Moore and R. B. Nielsen, *Curr. Opin. Chem. Eng.*, 2021, **31**, 100668.

2 P. Preuster, C. Papp and P. Wasserscheid, *Acc. Chem. Res.*, 2017, **50**, 74–85.

3 P. T. Aakko-Saksa, C. Cook, J. Kiviaho and T. Repo, *J. Power Sources*, 2018, **396**, 803–823.

4 Y. Sekine and T. Higo, *Top. Catal.*, 2021, **64**, 470–480.

5 S. Nagatake, T. Higo, S. Ogo, Y. Sugiura, R. Watanabe, C. Fukuhara and Y. Sekine, *Catal. Lett.*, 2016, **146**, 54–60.

6 J. H. B. Sattler, J. Ruiz-Martinez, E. Santillan-Jimenez and B. M. Weckhuysen, *Chem. Rev.*, 2014, **114**, 10613–10653.

7 Y. Okada, E. Sasaki, E. Watanabe, S. Hyodo and H. Nishijima, *Int. J. Hydrogen Energy*, 2006, **31**, 1348–1356.

8 X. Yang, Y. Song, T. Cao, L. Wang, H. Song and W. Lin, *J. Mol. Catal.*, 2020, **492**, 110971.

9 P. T. Aakko-Saksa, M. Vehkamäki, M. Kemell, L. Keskiväli, P. Simell, M. Reinikainen, U. Tapper and T. Repo, *Chem. Commun.*, 2020, **56**, 1657–1660.

10 A. P. Amrute, J. De Bellis, M. Felderhoff and F. Schüth, *Chem. – Eur. J.*, 2021, **27**, 6819–6847.

4154 | *Catal. Sci. Technol.*, 2025, **15**, 4143–4155

This journal is © The Royal Society of Chemistry 2025

11 C. Suryanarayana, *Prog. Mater. Sci.*, 2001, **46**, 1–184.

12 Y. Hu, B. Li, C. Yu, H. Fang and Z. Li, *Mater. Today*, 2023, **63**, 288–312.

13 H. Schreyer, R. Eckert, S. Immohr, J. De Bellis, M. Felderhoff and F. Schüth, *Angew. Chem., Int. Ed.*, 2019, **58**, 11262–11265.

14 J. De Bellis, H. Petersen, J. Ternieden, N. Pfänder, C. Weidenthaler and F. Schüth, *Angew. Chem., Int. Ed.*, 2022, **61**, e202208016.

15 M. Armengol-Profitós, A. Braga, L. Pascua-Solé, I. Lucentini, X. Garcia, L. Soler, X. Vendrell, I. Serrano, I. J. Villar-Garcia, V. Pérez-Dieste, C. Escudero, N. J. Divins and J. Llorca, *Appl. Catal., B*, 2024, **345**, 123624.

16 A. Rahemtulla, G. King, A. Gomez, N. Appathurai, A. Leontowich, R. Castle, N. Burns, C.-H. Kim, B. Moreno and S. Kycia, *J. Synchrotron Radiat.*, 2025, **32**, 750–756.

17 B. H. Toby and R. B. Von Dreele, *J. Appl. Crystallogr.*, 2013, **46**, 544–549.

18 S. Zhu, M. Scardamaglia, J. Kundsen, R. Sankari, H. Tarawneh, R. Temperton, L. Pickworth, F. Cavalca, C. Wang, H. Tissot, J. Weissenrieder, B. Hagman, J. Gustafson, S. Kaya, F. Lindgren, I. Kallquist, J. Maibach, M. Hahlin, V. Boix, T. Gallo, F. Rehman, G. D'Acunto, J. Schnadt and A. Shavorskiy, *J. Synchrotron Radiat.*, 2021, **28**, 624–636.

19 Y. Nakaya, M. Miyazaki, S. Yamazoe, K.-I. Shimizu and S. Furukawa, *ACS Catal.*, 2020, **10**, 5163–5172.

20 L. Chen, P. Verma, K. Hou, Z. Qi, S. Zhang, Y.-S. Liu, J. Guo, V. Stavila, M. D. Allendorf, L. Zheng, M. Salmeron, D. Prendergast, G. A. Somorjai and J. Su, *Nat. Commun.*, 2022, **13**, 1092.

21 K. Murata, N. Kurimoto, Y. Yamamoto, A. Oda, J. Ohyama and A. Satsuma, *ACS Appl. Nano Mater.*, 2021, **4**, 4532–4541.

22 M. D. Argyle and C. H. Bartholomew, *Catalysts*, 2015, **5**, 145–269.

23 R. Alcala, D. P. Dean, I. Chavan, C.-W. Chang, B. Burnside, H. N. Pham, E. Peterson, J. T. Miller and A. K. Datye, *Appl. Catal., A*, 2023, **658**, 119157.

24 Y. Mechiche, D. Lofficial, S. Humbert, M. Digne and A. Méthivier, *Powder Technol.*, 2024, **433**, 119179.

25 H. Iddir, V. Skavysh, S. Öğüt, N. D. Browning and M. M. Disko, *Phys. Rev. B: Condens. Matter Mater. Phys.*, 2006, **73**, 041403(R).

26 G. Bergeret and P. Gallezot, in *Handbook of Heterogeneous Catalysis*, Wiley-VCH, 2008, vol. 2, pp. 738–765.

27 J. Lee, I. Song and D. H. Kim, *ChemCatChem*, 2018, **10**, 1258–1262.

28 S. Yuan, Y. Duan, C. Yu, Z. Xiong, Y. Li, H. Wang, Y. Zhang and Y. Gao, *Mol. Catal.*, 2023, **535**, 112830.

29 H. Chermette, P. Pertosa and F. M. Michel-Calendini, *Chem. Phys. Lett.*, 1980, **69**, 240–245.

30 P. Mani, R. Srivastava and P. Strasser, *J. Phys. Chem. C*, 2008, **112**, 2770–2778.

31 X. Li, X. Wang, I. I. Sadykov, D. Palagin, O. V. Safonova, J. Li, A. Beck, F. Krumeich, J. A. van Bokhoven and L. Artiglia, *ACS Catal.*, 2021, **11**, 13041–13049.

32 A. von Weber and S. L. Anderson, *Acc. Chem. Res.*, 2016, **49**, 2632–2639.

33 Q. Liu and Z. Zhang, *Catal. Sci. Technol.*, 2019, **9**, 4821–4834.

34 A. Beck, X. Huang, L. Artiglia, X. Wang, P. Rzepka, D. Palagin, M.-G. Willinger and J. A. van Bokhoven, *Nat. Commun.*, 2020, **11**, 3220.

35 L. Qiu, F. Liu, L. Zhao, W. Yang and J. Yao, *Langmuir*, 2006, **22**, 4457–4884.

36 D. J. Morgan, *Surf. Interface Anal.*, 2015, **47**, 1072–1079.

37 T. Sekiya, S. Ohta, S. Kamei, M. Hanakawa and S. Kurita, *J. Phys. Chem. Solids*, 2001, **62**, 717–721.

38 E. Enríquez, A. del Campo, J. J. Reinosa, G. Konstantopoulos, C. Charitidis and J. F. Fernández, *J. Mater. Res. Technol.*, 2023, **26**, 2655–2666.

39 Z. Li, L. Deng, I. A. Kinloch and R. J. Young, *Prog. Mater. Sci.*, 2023, **135**, 101089.

40 M. Veres, S. Tóth and M. Koós, *Diamond Relat. Mater.*, 2008, **17**, 1692–1696.

41 M. C. Biesinger, *Appl. Surf. Sci.*, 2022, **597**, 153681.

42 H. Su, Y. Ye, K.-J. Lee, J. Zeng, B. S. Mun and E. J. Crumlin, *J. Catal.*, 2020, **391**, 123–131.

43 N. Bou-Orm, A. Iorgu, S. Daniele and N. Guilhaume, *Appl. Catal., A*, 2013, **467**, 414–420.

44 H. Li, M. Vrinat, G. Berhault, D. Li, H. Nie and P. Afanasiev, *Mater. Res. Bull.*, 2013, **48**, 3374–3382.

45 P. Wang, Z. Xu, T. Wang, Y. Yue, X. Baoa and H. Zhu, *Catal. Sci. Technol.*, 2020, **10**, 3537–3541.

46 Y. Tuo, Y. Meng, C. Chen, D. Lin, X. Feng, Y. Pan, P. Li, D. Chen, Z. Liu, Y. Zhou and J. Zhang, *Appl. Catal., B*, 2021, **288**, 119996.

47 Z. Dong, A. Mukhtar and H. Lin, *Top. Catal.*, 2021, **64**, 481–508.

This journal is © The Royal Society of Chemistry 2025

Catal. Sci. Technol., 2025, **15**, 4143–4155 | **4155**